

OTS: A One-shot Learning Approach for Text Spotting in Historical Manuscripts

Wen-Bo Hu^{a,b}, Hong-Jian Zhan^{a,b,*}, Cong Liu^c, Bing Yin^c, Yue Lu^{a,b}

^a*School of Communication and Electronic Engineering, East China Normal University, Shanghai, 200062, China*

^b*Shanghai Key Laboratory of Multidimensional Information Processing, Shanghai, 200241, China*

^c*iFLYTEK Research, iFLYTEK, Hefei, 230088, China*

Abstract

Historical manuscript processing poses challenges like limited annotated training data and novel class emergence. To address this, we propose a novel One-shot learning-based Text Spotting (OTS) approach that accurately and reliably spots novel characters with just one annotated support sample. Drawing inspiration from cognitive research, we introduce a spatial alignment module that finds, focuses on, and learns the most discriminative spatial regions in the query image based on one support image. Especially, since the low-resource spotting task often faces the problem of example imbalance, we propose a novel loss function called torus loss which can make the embedding space of distance metric more discriminative. Our approach is highly efficient and requires only a few training samples while exhibiting the remarkable ability to handle novel characters, and symbols. To enhance dataset diversity, a new manuscript dataset that contains the ancient Dongba hieroglyphics (DBH) is created. We conduct experiments on publicly available VML-HD, TKH, NC datasets, and the new proposed DBH dataset. The experimental results demonstrate that OTS outperforms the state-of-the-art methods in one-shot text spotting. Overall, our proposed method offers promising applications in the field of text spotting in historical manuscripts.

Keywords:

Text Spotting, Low-resource, One-shot Learning, Historical Manuscripts

*Corresponding author email: hjzhan@cee.ecnu.edu.cn

1. Introduction

To preserve cultural heritage, archives have been creating digital libraries by scanning or photographing historical manuscripts [1, 2]. However, the need for human summarization of scattered and limited information is still indispensable in deciphering and categorizing these ancient manuscripts. Given that these historical manuscripts typically comprise handwritten ancient characters, researchers have resorted to the use of optical character recognition (OCR) techniques [3, 4] to facilitate the digitization process of these invaluable manuscripts. Despite the significant progress made in Optical Character Recognition (OCR) methods, handling historical manuscript images poses a significant challenge due to several limitations.

(1) Open-set problem. Most methods only yield satisfactory results for trained categories, failing to cope with the open-set problem. This limitation is further aggravated by the absence of a complete alphabet in some manuscripts, with new characters being discovered during processing. While some unsupervised methods have surfaced to address the challenge of the open set problem [5, 6, 7], their effectiveness often leaves much to be desired.

(2) Low-resource scenario. With regard to those methods [8, 9, 10, 11] that rely on data for training, the demand for a substantial amount of annotated data poses an additional obstacle, given that historical manuscripts often feature a scant number of pages, rendering it challenging to obtain an ample number of training samples. Additionally, the log-tailed distribution of characters in ancient manuscripts exacerbates the problem of data sparsity, with some characters occurring only once. For the frequency of occurrence of all characters in the TKH dataset [13], a total of 1492 categories appeared, of which 436 category characters appeared only once.

(3) Eliminate additional layout analysis. Traditional methods typically require lines of text as input, necessitating pre-processing of images, layout analysis, and segmenting the character or text line image, which is time-consuming and prone to error accumulation [14, 15]. In contemporary times, there have been efforts to address page-level text-spotting tasks [16], but these approaches typically involve a two-step process that first detects text on the page and then utilizes a search-based method to extract the final results. However, these methods are susceptible to error propagation or necessitate a considerable amount of data to train a robust model [17, 18], the casual and disordered layout of antique manuscript images impedes the ability of such models to process these images efficiently in low-resource sit-

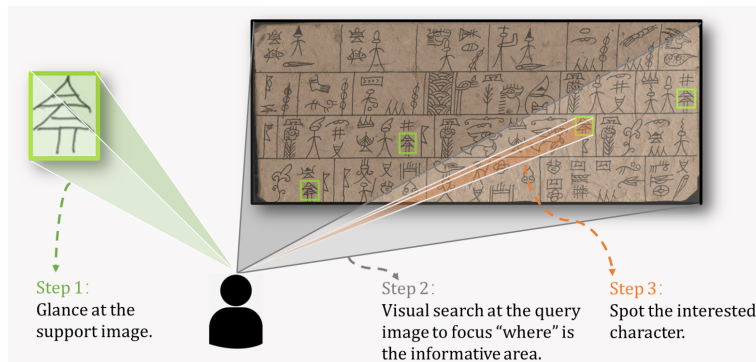


Figure 1: The human text spotting process with guidance can be roughly divided into three steps. (1) Support images serve as a reference. (2) The spotting area is narrowed to concentrate on potential regions of interest within the query image. (3) The desired character is spotted.

uations.

(4) Need more flexible application options. Some historical characters, including Dongba hieroglyphics or notary signs [19], these historical character not supported by input method editors, cannot be processed by most existing OCR methods [8, 9, 10, 11] that output textualized results.

Recently, cognitive research has demonstrated that humans possess a remarkable ability to recognize objects when provided with guidance [12], as exemplified by human visual searches in scenes with the aid of literacy cards, among other contextual cues (Figure 1). In this process, humans heavily rely on knowledge of the supporting images and contextual information. This dependence on support images (*e.g. literacy cards*) is believed to stem from the prefrontal cortex and is projected to lower-level visual cortex structures. Support information acts as a reference, directing attention to specific visual features. Meanwhile, spatial context information narrows the search area, guiding attention towards more relevant locations. The integration of both sources of information results in the identification of the region of interest.

For the sake of cultural preservation and for better handling of historical manuscripts, we draw inspiration from cognitive research on human learning and propose a one-shot learning model. One-shot learning aims to learn the characteristic patterns of a particular category and generalize them to unseen categories with just a single annotated example, rather than relying on a vast number of annotated examples. Specifically, our proposed one-shot learning model takes an input antique book page image and an example image of the

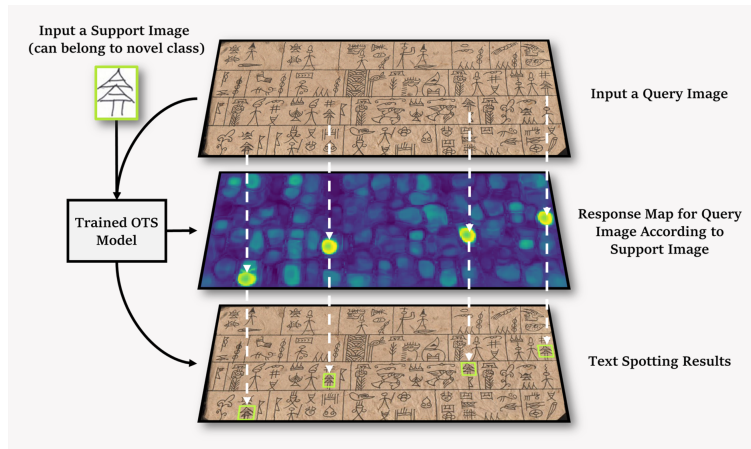


Figure 2: An illustration of the text spotting results on the DBH dataset based on one novel support image. The proposed framework can spot novel interested character categories conditioned with one support image. Dashed lines indicate correspondence, best view in color.

desired character class to spot all characters in that historical manuscript, even if the provided support image of the desired character belongs to an unseen category. The model requires only a small number of samples for training, which can produce the desired results in page-level, as shown in Figure 2. To address the problem of example imbalance, we propose a novel loss function called torus loss, which makes the embedding space of the distance metric more discriminative. Our proposed approach can handle varying characters and symbols such as hieroglyphics, Arabic, Chinese, and notary signs appearing on historical manuscripts. The proposed method provides a more flexible and efficient solution for historical manuscript text spotting. The contributions of our work can be summarized as follows:

(1) One-shot and human-like. We propose a flexible one-shot text spotting model that accurately and reliably spots novel characters with just one annotated support sample. The innovative dual spatial attention block emulates the human cognitive process, extracting valuable information from the support set to guide the model’s focus on key regions in the query image.

(2) Low-resource scenario and page-level. It requires only a small number of training samples and eliminates the additional fine-tuning step required by previous approaches. A novel loss named torus loss is proposed, which can focus on the hard examples and learns a distance metric for better text spotting in low-resource scenarios. Our approach eliminates the need for

additional layout analysis of historical manuscript images, enabling page-level text spotting and making our scheme more applicable to realistic scenarios.

(3) New datasets. As a contribution to the community, we have repurposed some publicly available datasets. Additionally, we have introduced a new dataset of ancient Dongba script manuscripts, which consists of hieroglyphic characters and provides researchers studying text spotting in low-resource situations with a valuable resource.

2. Related work

2.1. Text Spotting

Certain segmentation-based methods [20, 21, 22] assume that the dataset is already partitioned into text lines or words, thereby rendering these methods more akin to an image retrieval task, where the goal is to retrieve the most relevant images in the dataset. Additionally, some text spotting techniques typically detect each text instance using a trained detector, then identify the cropped text region using a sequence decoder [23, 24]. However, such a strategy undermines performance robustness since the detection and recognition phases are separated, and the error from the recognition model cannot be used to optimize the detector. In recent times, there has been growing interest in end-to-end scene text detection and recognition, which offer the benefit of achieving both detection and recognition tasks by sharing the acquired features between the two steps [17, 18, 25, 26, 27]. Nevertheless, these methods usually require an extensive corpus of data to enable adequate training and are unable to identify new categories. [5] using a sliding window scheme with deep features to accomplish the text spotting task is also one of the solutions. This approach can be seen as a kind of unsupervised learning, so there is no open-set problem, unfortunately, this sliding window based approach usually does not achieve the best results. [28] propose a word spotting method based on the "query-by-string" approach, which allows the user to retrieve all instances of a given string in a document image. However, while this method can be effective for seen characters, it does not address the challenge of mining unseen characters, which is particularly relevant for ancient texts.

Furthermore, many ancient texts do not yet have a complete lexicon, and consequently, there are no corresponding input method editors, making it challenging to identify and retrieve specific strings in these documents. Historical manuscripts often pose a significant challenge due to their limited

availability of annotated images. For instance, the Pascal VOC dataset [29], widely utilized in few-shot object detection, includes a meager 1.6 categories and 2.9 instances per image on average. In stark contrast, the data distribution of historical manuscript images is significantly broader, as evidenced by the TKH dataset, which boasts an average of 72.5 categories and 323.8 character instances per image. Drawing inspiration from few-shot object detection and to address the challenge of limited data in historical manuscripts, Sougibui et al. [30] design a few-shot character recognition method that aims to overcome the low-resource problem and enable the model to recognize unseen alphabets. Nonetheless, [30, 31] are only applicable to text line images, necessitating prior layout analysis to segment the original page into lines. In contrast, our proposed method can process page images without requiring additional layout analysis.

2.2. Few-shot Object Detection

In the realm of few-shot learning, extant techniques have predominantly been designed for classification tasks. Optimization-based methods nimbly assimilate novel categories via gradient-based optimization on a paltry number of annotated samples [32, 33, 34]. Conversely, the metric-based learning paradigm seeks to glean a common feature space and demarcate categories based on a distance metric [35, 36]. One-shot learning [37, 38] stands as an extreme manifestation of the few-shot learning paradigm, characterized by each novel encountered category boasting a singular labeled example.

The goal of few-shot object detection is to discern the location and identity of objects in query images with the aid of a limited set of labeled support images [39, 40, 41, 42, 43, 44, 45, 46, 47]. To circumvent the open-set problem, a two-stage approach is often employed, in which the model is first trained on base categories and then fine-tuned on a small number of samples for novel categories. However, this approach can lead to confusion between novel and base categories, resulting in decreased model efficacy as the number of novel categories increases [41, 42, 44, 47]. In situations where training samples are scarce, some approaches may struggle to locate regions of interest for novel objects, particularly those with unlearnable shape priors and fine-tuned RPNs [48]. However, certain methods have demonstrated the ability to detect new categories without fine-tuning, such as OS2D [40], which uses a similarity map and learned dense matches to establish correspondence between support and query images. This model excels at learning

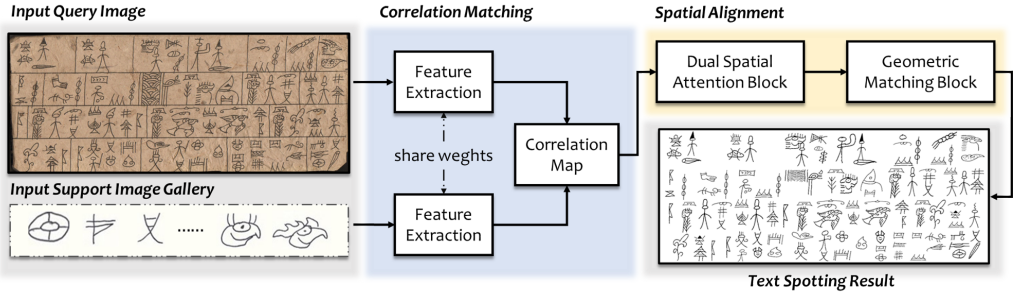


Figure 3: The overall framework of OTS. Based on the feature extracted by the backbone network, the correlation matching module computes the correlation map to match the pair of individual feature maps, while the spatial alignment module predicts the localization boxes and spotting results. The spotting result is the pasting of the character image from the support image gallery onto a blank image of the same size as the input query image.

pixel-matching relations between the support and query images, thereby allowing it to handle novel classes without fine-tuning. Our proposed model is also based on dense correlation matching features. However, in few-shot tasks with a small number of samples, attention must be explicitly directed toward the target item (based on the support image) since most visual prediction models exhibit free-viewing behavior. Compared with OS2D, our model design strategy is closer to the human cognitive process, despite the different objectives of our task. Additionally, we discuss the spotting process in low-resource scenarios and propose a new loss function for it. CoAE [42] is also a method that does not require fine-tuning, proposing a non-local RPN to tackle the problem of one-shot object detection. However, RPN-based methods often use a predefined set of anchor boxes with different scales and aspect ratios to generate region proposals, which may not be able to capture the small variations in size and aspect ratio of small objects, especially in historical manuscripts.

3. Proposed method

We treat recognition as a one-shot text-spotting task: by providing only one sample of each character type in the support image gallery, the model could locate the characters in the manuscript. As in Figure 3, the proposed model consists of two modules: correlation matching module and spatial alignment module. In the correlation matching module, the feature extractor first extracts the features of the query image and support image. The

relationship between feature map pairs is calculated to obtain the correlation map. After that, the spatial alignment module will learn the transformation parameters that allow the model to gain the ability to localize the support image on the query image. Since some characters on ancient manuscripts are not yet able to use the input method editor, we select items from the support image gallery $S_{gallery} \in C_{base} \cup C_{novel}$ and pasted them onto a blank image with the same size as the query image $I_q \in T_{test}$ to create a new standard image to be displayed as the result of text spotting.

3.1. Problem Formulation

The query sets Q are page-level images of historical manuscripts, and the support sets S are images of individual characters. In the process of training, we have the training set $T_{train} = \{(Q_n, S_i), S_i \in C_{base}\}$, and utilize the data from the validation set $T_{val} = \{(Q_n, S_j), S_j \in C_{novel}\}$ to select the optimal model. Note that, the character classes of the database are divided into two disjoint parts $C_{base} \cap C_{novel} = \emptyset$, where C_{base} denotes the base category and C_{novel} denotes the novel category. During the evaluation phase, we have additional new data $T_{test} = \{(Q_m, S_j), S_j \in C_{novel}\}$.

3.2. Correlation Matching

3.2.1. Feature Extractor

For the input support and query images, (I_s, I_q) , are passed through two feature extraction CNN branches with shared weights. Since most of the antique manuscripts are insufficient to train the network from scratch, the feature extractor can only gain experience from the base category for the one-shot task. It cannot get targeted training from the novel category. For each input support image I_s^i , the feature map $f_s^i \in R^{h_s^i \times w_s^i \times D}$ obtained after backbone, is uniformly resized to the same size $f_s^i \rightarrow f_s \in R^{h_s \times w_s \times D}$. Finally, the feature extraction networks extract the support feature $F(I_s) = f_s \in R^{h_s \times w_s \times D}$ and query feature $F(I_q) = f_q \in R^{h_q \times w_q \times D}$, respectively, where F represents the backbone, $h \times w$ is the spatial resolution and D is the channels.

3.2.2. Correlation Map

To ensure the model can have sufficient generalizability to unseen categories. Intuitively, the model must fully avail of the reference information provided by the support image. A common strategy for computing the correlation map is to match a pair of individual feature maps using normalized cosine similarity [49, 50]. Given a pair of individual features $f_s \in R^{h_s \times w_s \times D}$

and $f_q \in R^{h_q \times w_q \times D}$ of support and query images, the correlation map is computed as:

$$C_{abkl} = \phi(f_q, f_s) = \frac{f_q \cdot f_s^T}{\|f_q\| \|f_s\|} \in R^{h_q \times w_q \times h_s \times w_s}, \quad (1)$$

where $\phi(\cdot)$ means cosine similarity, and C_{abkl} denotes the matching score between the (a, b) -th position in query feature map and (k, l) -th position in support feature map. The result is thus a 4D tensor that captures the similarities between all pairs of spatial locations.

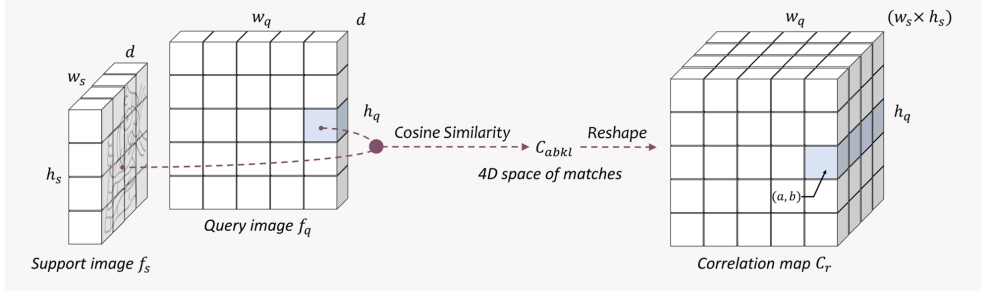


Figure 4: Correlation map computation with a pair of individual features. After extract the image descriptors f_s and f_q for images I_s and I_q , respectively. Subsequently, all pairs of individual feature matches f_s^{kl} and f_q^{ab} are represented in the 4D space of matches (a, b, k, l) , with the matching score stored in the 4D correlation tensor. We then reshape this 4D tensor to a 3D tensor with dimension h_q , w_q and $(h_s \times w_s)$, enabling us to construct a correlation map. At a particular spatial location (a, b) , the correlation map C_r provides an aggregation of all the similarities between $f_q(a, b)$ and all f_s .

3.3. Spatial Alignment

The spatial alignment module consists of two blocks, the dual spatial attention (DSA) block and the geometric matching (GM) block. The primary purpose of the dual spatial attention block is to find, focus and learn discriminative spatial regions on support/query images. And the primary purpose of the geometric matching block is to find the spatial mapping relationship between the support image and the query image. These two blocks stimulate each other, which helps to get more accurate text spotting results.

Unlike the geometric matching methods [51, 52, 53] that have been utilized for correspondence learning, the number of characters that appear in the antique manuscripts is very large, the character shapes are usually tiny,

and the character-to-character constructions are very similar. For this reason, we develop a spatial alignment module to facilitate locating the position of the character instance given by the support image on the query image at the dense pixel level. Specifically, the spatial alignment module aims to find spatial correspondence between a pair of support and query images. To achieve this, the obtained 4-dimensional correlation map, can be reshaped to a 3-dimensional tensor with dimensions h_q, w_q and $(h_s \times w_s)$, *i.e.*, $C_r = R^{h_q \times w_q \times (h_s \times w_s)}$. The reshaped correlation map C_r can be considered as a dense $h_q \times w_q$ grid with $(h_s \times w_s)$ -dimensional local features as shown in Figure 4.

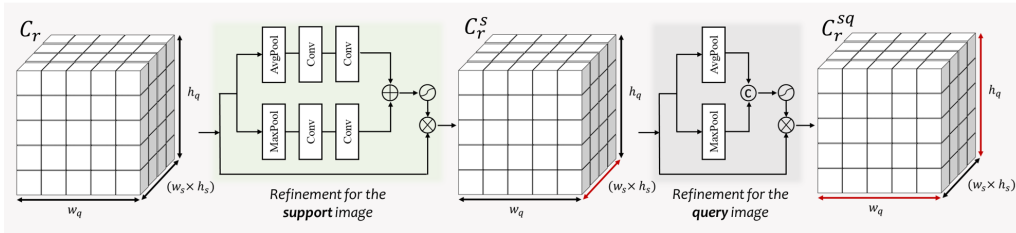


Figure 5: Flowchart of dual spatial attention block. Given the correlation map C_r from the correlation matching module, the first step is to attention to the dimension $d = (h_s \times w_s)$ of the correlation map, which can be regarded as a refinement for the support image. The next step is to attention to the dimensions w_q and h_q of the correlation map, which can be regarded as a refinement for the query image.

3.3.1. Dual Spatial Attention Block

When humans are guided based on support images, during a glance, human will remember the most critical salient regions that contribute to the visual spotting. Besides, when we need to find a character in a page of a book, blank areas or illustrations are ignored in the process of visual spotting. Thus, the spotting area is narrowed to concentrate on potential regions of interest within the query image, which means human will focus potential discriminative area.

Step 1. Refinement for the support image. Given the correlation map $C_r \in R^{h_q \times w_q \times d}$ by the correlation matching module, where $d = (h_s \times w_s)$. The correlation map not only contains the all information of the support and query image, but also the simiaity between two images are also include. For correlation map C_r , each channel d_j of C_r represents the correlation of the j -th pixel on the feature map $\{f_s\}_j$ with f_q , we produce a 1d spatial-wise

attention map to focus "where" is meaningful localization in the support image, as shown in Figure 5. We first feed the obtained C_r into the dual spatial attention block to find regions with key discriminative properties in the support image. Aggregating the spatial information of the correlation map C_r by using average-pooling and max-pooling operations, generating two different spatial context descriptors f_c^{avg} and f_c^{max} . After that, features pooled by each pooling layer are then passed through the support refinement network, which consists of two convolutions layer with kernel size 1. The purpose of support refinement network is to generate the inter-channel relationship of C_r , which means find the most prevalent critical areas of the support image. Then the element-wise summation is used to merge the results which have:

$$M_s = \sigma_s(W_1(W_0(AvgPool(C_r))) + W_1(W_0(MaxPool(C_r)))), \quad (2)$$

where $W_0 \in R^{d \times (d/\tau)}$, $W_1 \in R^{(d/\tau) \times d}$ are parameters of convolutions, σ_s represents the sigmoid activation function and τ is the reduction ratio. Then multiply $M_s \in R^{1 \times 1 \times d}$ with the correlation map C_r , expressed as:

$$C_r^s = M_s \otimes C_r, \quad (3)$$

where C_r^s captures the key points in spatial dimension of the support image and \otimes denotes element-wise multiplication.

Step 2. Refinement for the query image. Note that, at a particular position (a, b) of C_r^s contains the similarities between $f_q(a, b)$ and all the features of f_s . As illustrated in Figure 5, we also generate a 2d spatial attention map to focus "where" is the positional informative key point for the query image. By using average-pooling and max-pooling operations along the channel dimension and concatenating the pooled features. Then a convolution layer is applied to generate the spatial attention map:

$$M_q = \sigma_q(Conv([AvgPool(C_r^s); MaxPool(C_r^s)])), \quad (4)$$

where σ_q represents the sigmoid activation function, and $Conv$ represents a convolution operation with the filter size of 3×3 . To obtain the final refined features, we multiply $M_q \in R^{h_q \times w_q \times 1}$ with C_r^s , which can be expressed briefly as:

$$C_r^{sq} = M_q \otimes C_r^s, \quad (5)$$

where C_r^{sq} captures the key points in the spatial dimension of the query image and retains the key points focus of the support image.

3.3.2. Geometric Matching Block

For the obtained attention correlation map C_r^{sq} , the geometric matching block is applied to find the spatial correspondence between the I_s and I_q . To achieve this, we optimize a transformation function $W_\theta : \mathbb{R}^2 \rightarrow \mathbb{R}^2$, where θ denotes the alignment parameter. The spatial coordinates between I_q and I_s can be found by $(k', l') = W_\theta(k, l)$, where (k', l') are the corresponding spatial coordinates of (k, l) in f_q . Similar [54, 55], the geometric matching block consists of two consecutive convolutional layers without padding and stride equal to 1, with batch normalization and ReLU connected between the two convolutional layers, and finally a fully-connected layer to regress the alignment parameter θ . The goal of the GM block is to find the best parameters $\hat{\theta}$:

$$\hat{\theta} = \arg \max_{\theta} \sum_{(k,l)} \phi(f_{W_\theta(k,l)}^q, f_{k,l}^s), \quad (6)$$

where $\sum_{(k,l)} \phi(f_{W_\theta(k,l)}^q, f_{k,l}^s)$ means the summation of the feature similarities between the support feature and the regions corresponding to those on query image obtained through the 2D geometric transformation. After that, the obtained transformations are input to the grid sampler to generate a grid of points, which is aligned with the support image at each location of the query image.

Note that, the process of location is already done implicitly in the alignment process, by extracting the position frames based on the maximum and minimum values of the obtained grid tensor, by simply outputting a square tight bounding box based on the transformed grid points. The spotting score can be obtained by computing $\sum_{(k,l)} \phi(f_{W_\theta(k,l)}^q, f_{k,l}^s)$, *i.e.*, the similarity score of the local region on the query image feature $f_{W_\theta(k,l)}^q$ to the input support image feature $f_{k,l}^s$.

3.4. Loss Function

The loss function needs to construct the training objective from both localization and spotting [40, 41, 56].

Localization Loss. In this study, the smooth L_1 loss is used for localization:

$$l_{loc}(v, t) = \begin{cases} \sum_p \frac{1}{2}(v_p - t_p)^2, & \text{if } |v_p - t_p| < 1. \\ \sum_p |v_p - t_p|^{-\frac{1}{2}}, & \text{otherwise.} \end{cases} \quad (7)$$

where $v = (v_x, v_y, v_w, v_h)$ denotes the frame coordinates of GT and $t = (t_x, t_y, t_w, t_h)$ denotes the frame coordinates obtained by prediction.

Spotting Loss. Our task has an inherent difficulty to balance positive and negative samples. Ideally, the distance metric of positive examples is infinite, while the distance metric of negative examples should be close to 0. To separate positive and negative samples, we want that the distance metric of positive samples should be greater than margin m_{pos} , while the distance metric of negative samples should be less than margin m_{neg} . Therefore, the hinge-embedding loss with margins can be written as follows:

$$l_{pos}^i = \max(m_{pos} - s_i, 0), \quad (8)$$

$$l_{neg}^i = \max(s_i - m_{neg}, 0), \quad (9)$$

where m_{pos} and m_{neg} are the positive and negative margins, and $s \in [-1, 1]$ is the spotting score. To separate positive and negative examples, the contrastive loss [57] is considered:

$$L_c = \sum_i (l_{pos}^i + l_{neg}^i). \quad (10)$$

To acquire discriminative embeddings through contrastive learning, [58] introduced the ranked list (RL) loss which features the ability to adaptively mine negative samples by providing a weighting parameter. The RL loss can be formulated as follows:

$$L_{rl} = \sum_i (l_{pos}^i + w_i l_{neg}^i), \quad (11)$$

where w_i is defined as $w_i = \exp(T \cdot (s_i - m_{neg}))$, $s_i - m_{neg} > 0$, and T is the temperature parameter which controls the degree of weighting negative examples. However this loss function can not deal with the hard examples.

The ranked list (RL) loss is designed to assign different weights to negative examples and measure the distance between s_i and m_{neg} , thereby alleviating the issue of imbalanced examples. Figure 6(a) depicts the data distribution before training. During training (Figure 6(b)), examples C and D are expected to incur a large loss from the RL loss (Eq. (11)). However, the hard examples A and B within the margin gap will receive a relatively small loss, which is suboptimal for achieving the desired separation between positive and negative examples. To address this issue, it is desirable for the values of

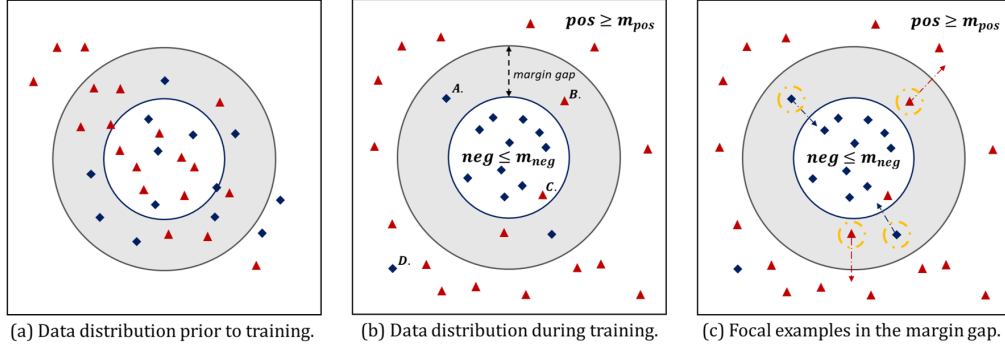


Figure 6: Data distribution analysis. (a) Prior to training, the data may be distributed in a complex and nonlinear fashion, with no clear separation between positive and negative examples. (b) During training, the model may be able to identify some patterns and achieve a degree of separation between positive and negative examples. Some examples may still remain in the margin gap, where the decision boundary is unclear and further optimization is needed to achieve greater separation. (c) To achieve optimal performance, we expect the values of positive examples to be greater than the margin m_{pos} , while the values of negative examples should be less than the margin m_{neg} .

positive examples to exceed the margin threshold m_{pos} , whereas the values of negative examples should fall below the margin m_{neg} . Accordingly, we aim to focus on the challenging examples in the margin gap and give them more attention to achieve a clear separation between positive and negative examples. For the example in the margin gap, we set:

$$g_i = \begin{cases} m_{pos}, & s_i \geq m_{pos} \\ s_i, & m_{neg} < s_i < m_{pos} \\ m_{neg}, & s_i \leq m_{neg} \end{cases} \quad (12)$$

Then the improved hinge-embedding loss with margins can be formulated as follows:

$$l_{pos'}^i = l_{pos}^i - \log\left(\frac{g_i}{m_{pos}}\right), \quad (13)$$

$$l_{neg'}^i = w_i l_{neg}^i - \log\left(\frac{m_{pos} + m_{neg} - g_i}{m_{pos}}\right), \quad (14)$$

where w_i is also defined as $w_i = \exp(T \cdot (s_i - m_{neg}))$, $s_i - m_{neg} > 0$. When the s_i falls in the margin gap, both positive and negative examples receive extra loss, which help to further separate them. For the $-\log(g_i/m_{pos})$, we want the value of positive examples to exceed the margin threshold m_{pos} . If the spotting

score is greater than m_{pos} , it meets the optimization goal and no further optimization is necessary. Similarly, for the $-\log((m_{pos} + m_{neg} - g_i)/(m_{pos}))$, we expect the value of negative examples to fall below the margin threshold m_{neg} .

The new loss function which improved RL loss which called torus loss can be formulated as follows:

$$L_{torus} = \sum_i (l_{pos'}^i + w_i l_{neg'}^i). \quad (15)$$

The torus loss not only addresses the issue of hard examples in the margin gap but also helps to mitigate the impact of example imbalance. Therefore, we can use this function as the spotting loss.

Training Objective. Finally, the total loss of our model can be expressed as:

$$L = \lambda L_{loc} + L_{torus}, \quad (16)$$

where $L_{loc} = \sum_i l_{loc}(v_i, t_i)$ and $L_{torus} = \sum_i (l_{pos'}^i + w_i l_{neg'}^i)$. λ is a hyperparameter that balances the importance of the two loss terms.

4. Experiments

4.1. Datasets

In order to thoroughly evaluate the efficacy of our proposed method and make a meaningful contribution to the research community, we have meticulously curated the currently available public datasets to provide a more comprehensive and specific framework for utilizing them in the context of one-shot text spotting. Moreover, we introduce a novel dataset of historical manuscripts that feature atypical character shapes, which is particularly suited to the one-shot text spotting task. The details regarding the number of image samples present in the training and evaluation datasets for the four datasets are presented in Figure 7.

Dongba Hieroglyphics dataset (DBH) is a newly proposed dataset in this work, which includes Dongba characters, an ancient hieroglyphic script that is invented by the ancestors of the Naxi minority in China. Dongba pictographs are a valuable part of history and literature and have been listed as "Memory of the World" by UNESCO. Despite the discovery of new characters through studying historical Dongba manuscripts, the total number of semantically distinct Dongba characters remains unknown. Therefore,

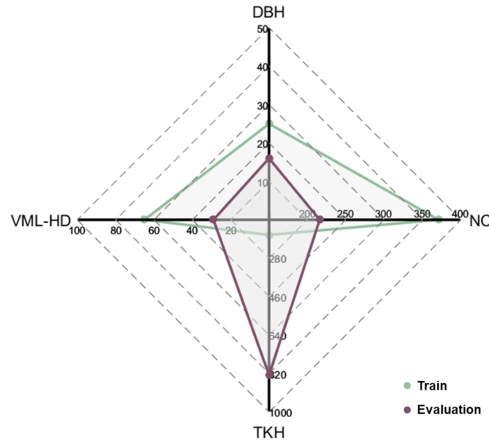


Figure 7: Summary of the data distribution of four datasets. The images in the validation set are also included in the "Train". For example, during the training phase, only 311 images from the Notary training set are used for training, and the remaining 60 images are used as the validation set to help select the best model.

the task of text spotting in Dongba historical manuscripts can be viewed as an open-set problem, where accurately spotting characters belonging to novel classes can aid in deciphering and summarizing historical characters in ancient manuscripts. To address this challenge, we collect data from the Dongba sutras, annotated and summarized the data, and created a dataset with 3633 bounding boxes and 253 categories. Since one-shot tasks usually require additional sets of support images, professionals hand-wrote an additional 253 characters independent of the original images, and used these hand-written images as the support image set to avoid controversy. The dataset is expected to facilitate future research on one-shot text spotting in historical manuscripts and an enhanced version with a larger number of images is planned for release in the future.

VML-HD dataset (VML) [59] is a valuable resource for researchers working with historical Arabic documents. It comprises 94 images, with a total of 1770 unique character categories, of which 150 are randomly selected as novel categories. The training set includes 65 images, and the remaining 29 images are used for testing.

Tripitaka Koreana in Han dataset (TKH) [13] consists of scanned images from Chinese antiquarian books. It contains a total of 999 images, with 1492 different character categories. For this dataset, 171 images are chosen for training, and 828 images are reserved for testing.

Notary Charters dataset (NC) [19] is a collection of manuscripts from classical and medieval eras, consisting of 388 different categories of notary charters. Among these, 311 categories appear only once, and are thus selected for training. The remaining images are reserved for testing, with 77 categories chosen as novel categories.

4.2. Implementation details

We employ a data augmentation strategy that involves randomly cropping patches of size 800×800 to all query images. This approach not only prevents over-fitting but also allows the model to learn from input query images containing multiple characters and categories. Besides, we iteratively adjusted it based on the results obtained from the validation set and selected the model that achieved the best performance. For the training objective function, the $m_{pos} = 0.6$ and $m_{neg} = 0.5$, and the hyperparameter λ is set to 0.2. Our implementation of the one-shot text spotting (OTS) model is based on PyTorch 1.9 and trained using the Adam optimizer [60] with a learning rate of $1e-4$ and a momentum of 0.9 on one Nvidia GeForce RTX 3090. We consider the third blocks of the pre-trained ResNet-50 network [61] on ImageNet [62] are used as the feature extractor. We apply an affine transformation with a 6-degree-of-freedom linear transformation for the geometric matching. To evaluate the performance of our model, we use the standard Pascal VOC metric [29], following the mainstream setting of using mean average precision (mAP) and recall as the evaluation metrics. We use an intersection-over-union (IoU) threshold of 0.5 for mAP evaluation. All datasets and code will be publicly available¹.

4.3. Results

4.3.1. Comparison Baseline

Initially, it is hypothesized that certain one-shot object detection methods could also address the task of one-shot text spotting. To test this hypothesis, we retrained some popular few-shot object detection methods [41] using the four datasets previously summarized. Unfortunately, the experimental performance fell short, struggling to surpass 8% mAP. This is mainly due to the fact that historical manuscripts usually comprise a large number of characters, frequently exceeding 100 different categories. These characters possess

¹<https://github.com/infinite-hwb/ots>

similar glyphs or significantly vary in scale, thereby presenting significant challenges for one-shot text spotting. Although we attempted to use the popular object detector method Faster RCNN [48], the paucity of training data made it difficult to achieve meaningful results. Therefore, we opted to use OS2D [40], a dense correlation matching feature-based method for one-shot object detection, as our baseline. This approach trains the transform network from a model pre-trained with weak supervision. As there has been no prior research on one-shot text spotting, we adapted OS2D [40] to suit our historical manuscripts by fine-tuning the method’s parameters and using the same data augmentation scheme as our proposed method. Although CoAE’s intended purpose is to detect objects in natural scenes, it has been included as one of the comparison methods for its efficacy in one-shot object detection using the RPN approach in recent years. To make a fair comparison, we have also added multi-scale pyramids to the training and testing of CoAE. Furthermore, we have experimented with DSW [5], a classic unsupervised approach for text spotting based on the "sliding window" technique, and reproduced its main idea by directly mapping the feature map of the support image as a convolution on the query image after extracting the features using a Siamese network with specifications identical to our method.

4.3.2. Statistical results and analysis

The statistical results are shown in Table 1, where the *Novel* column indicates the performance of the unseen category on the test set, the *Base* column denotes the performance of the base category that appears on the test set, and the *HM* column indicates the harmonic average performance of base and novel classes. It is worth noting that, in Table 1, the test set of the NC dataset does not contain base categories, and hence, we only evaluate the new classes in the test set. To alleviate memory pressure on the computer, we partition the test set of the TKH dataset into two subsets, Set 1 and Set 2, with 390 and 438 test images, respectively. During evaluation, the support image is resized while preserving its aspect ratio for all compared methods. A pyramid of five levels (0.4, 0.6, 0.8, 1.0, and 1.2 times the dataset scale) is used for the query image. The DBH dataset had a scale of 2500, the VML dataset had a scale of 4000, the TKH dataset had a scale of 5500, and the NC dataset had a scale of 4000.

From the experimental results, it is evident that our method achieves the best recall score in all datasets, indicating that our method exhibits a low tendency to miss text spotting. Furthermore, our proposed method

Table 1: Quantitative evaluation on DBH, VML, TKH and NC. Note that, \ denotes the test set of the NC does not contain the base categories, and hence, we only evaluate the novel classes. The best results are highlighted in **bold**.

Dataset	Method	Strategy	Novel		Base		HM	
			mAP	Recall	mAP	Recall	mAP	Recall
DBH	DSW[5]	unsupervised	51.70	59.64	39.08	35.76	44.51	44.71
	CoAE[42]	supervised	62.64	60.36	72.55	93.55	67.23	73.37
	OS2D[40]	supervised	98.08	99.29	89.22	94.76	93.44	96.97
	OTS(Ours)	supervised	99.85	100.0	91.74	95.17	95.62	97.53
VML	DSW[5]	unsupervised	62.77	74.15	20.70	46.83	31.13	57.40
	CoAE[42]	supervised	39.07	60.17	27.30	53.07	32.14	56.39
	OS2D[40]	supervised	94.39	98.31	55.31	52.45	69.75	68.40
	OTS(Ours)	supervised	100.0	100.0	66.59	70.57	79.94	82.75
TKH Set 1	DSW[5]	unsupervised	42.63	92.02	41.70	83.71	42.16	87.67
	CoAE[42]	supervised	36.74	47.30	58.81	85.92	45.23	61.01
	OS2D[40]	supervised	88.05	99.60	89.31	95.72	88.68	97.62
	OTS(Ours)	supervised	90.20	99.65	90.51	95.78	90.35	97.67
TKH Set 2	DSW[5]	unsupervised	37.95	88.68	36.22	82.03	37.06	85.22
	CoAE[42]	supervised	35.78	45.73	54.67	81.74	43.25	58.65
	OS2D[40]	supervised	86.20	98.35	85.53	95.96	85.86	97.14
	OTS(Ours)	supervised	88.06	99.52	87.50	96.26	87.78	97.86
NC	DSW[5]	unsupervised	59.60	66.06	\	\	\	\
	CoAE[42]	supervised	85.82	93.58	\	\	\	\
	OS2D[40]	supervised	76.15	77.92	\	\	\	\
	OTS(Ours)	supervised	92.14	96.79	\	\	\	\

outperforms the other compared methods in terms of mAP scores. It is important to note that the sliding window method can be considered as an unsupervised technique, and we provide the correct aspect ratio of the support image feature maps for the sliding window approach. However, the results demonstrate that the performance of the unsupervised method based on sliding windows is inferior to that of the supervised learning method, such as OS2D and OTS. In addition, we observe that sometimes the unsupervised method of DSW outperforms the supervised method of CoAE, which we attribute to the limited amount of data that does not allow CoAE to be fully learned. When considering the perspective of data distribution, the DBH and NC datasets exhibit a more dispersed inter-class distribution of characters

appearing in the manuscript images, while the VML and TKH datasets have a more compact inter-class distribution and smaller character size, which CoAE cannot cope with. In the case of the VML and TKH datasets, numerous similar characters are present, and our OTS method outperforms the baseline method.

We observe that CoAE achieves better performance on the base class than the novel class, whereas OTS exhibits exceptional results on processing novel classes but with some degradation on the base categories. Nonetheless, our proposed method still outperforms other methods. During the training process, OTS learns to match potential regions of the query image with the support character instance, rather than accumulating class-specific knowledge. This learning strategy enables the model to perform effectively with a limited number of training samples, which is particularly important in the context of historical manuscript data with small and sparse datasets. By eschewing the requirement for an extensive corpus of training samples, the proposed method stands out as a superior approach to other one-shot methods, which necessitate a more significant volume of samples to achieve comparable results. As such, the proposed OTS offers a practical solution to the challenge of one-shot text spotting in the realm of historical manuscripts.

Rotational Disturbance. Our proposed method exhibits remarkable robustness to slight rotation variations in test images, without the need for rotation augmentations during the training process. We conducted rotation disturbance on test images, varying from 0° to 15° at 2.5° intervals. As illustrated in Figure 8, our method outperforms the comparison methods in handling rotated test images, with only minimal performance degradation as the rotation angle increases. In contrast, the RPN-based CoAE model experiences a rapid decline in performance when faced with rotation disturbances. The performance of OS2D model exhibits slow degradation as the rotation angle of the query image increases. The unsupervised sliding window-based method appears to have minimal impact on rotation disturbances. Notably, digitized images of ancient manuscripts may have slight rotation variations resulting from the scanning process. Our method demonstrates consistent high performance even in the presence of such rotational disturbances, thus confirming its robustness and practicality.

4.3.3. Qualitative results and analysis

Figure 9 illustrates visualizations of some qualitative results on the VML dataset, enabling a facile comparison of the proposed method with OS2D,

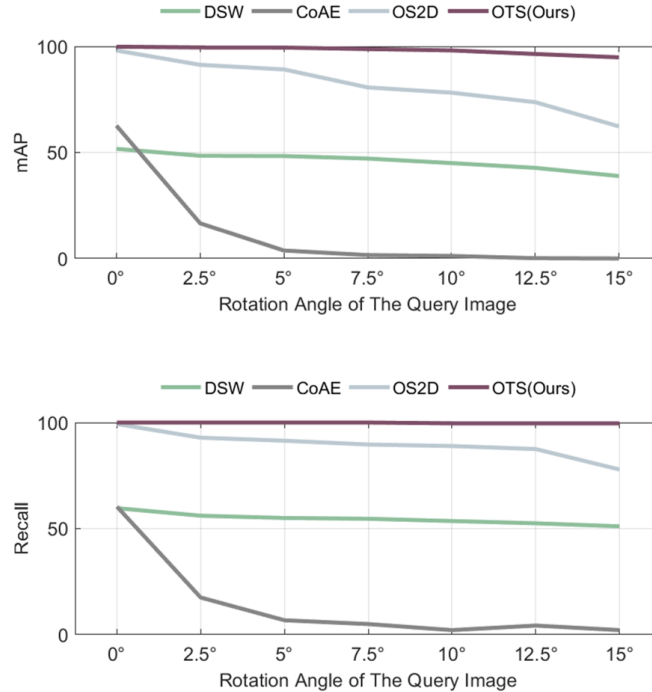


Figure 8: Quantitative evaluation on DBH Novel with different angles of rotation on query images.

which is the most competitive method. The VML dataset presents unique challenges due to the copious number of character classes, including concatenated strokes. Our empirical results demonstrate that our proposed approach outperforms OS2D, attesting to the superior efficacy of our method. Moreover, the quality of the support image significantly impacts the localization and spotting performance. In order to showcase the robustness of our approach to varying image quality, we present visual results with support images of low quality in Figure 10. Impressively, our method consistently achieves top-notch performance, even when the support image is blurred, as depicted in the first row of Figure 10. Notably, both OS2D and OTS demonstrate accurate character spotting when the support image is affected by illumination, as demonstrated in the second row of Figure 10. Furthermore,



Figure 9: Example results on VML-HD dataset. The leftmost column shows the ground truth, and the red box is the support image. All prediction boxes are shown in green. Best view in color and zoom in.

we provide a demo video^{2 3} that effectively demonstrates the effectiveness of our proposed method, comprising several brief clips. In each clip, an image is randomly selected from the test set, and a rectangular box of interest (typically a character or word) is delineated and utilized as the support image. Subsequently, various images from the test set are chosen as query images, and the results achieved using our method are presented in the latter half of the video.

Spotting Novel Combination Characters. The proposed approach offers the flexibility to handle diverse and evolving application scenarios by allowing for the spotting of novel classes. In particular, we define a "word" as a combination of characters belonging to a novel class, when a single character sample is used as the support image during training. The extensive annotation required to count which characters can form a word makes quantitative comparisons challenging. As a result, we provide

²<https://youtu.be/8GRDOxCDMjw>

³<https://www.bilibili.com/video/BV12x4y1K7MX/>

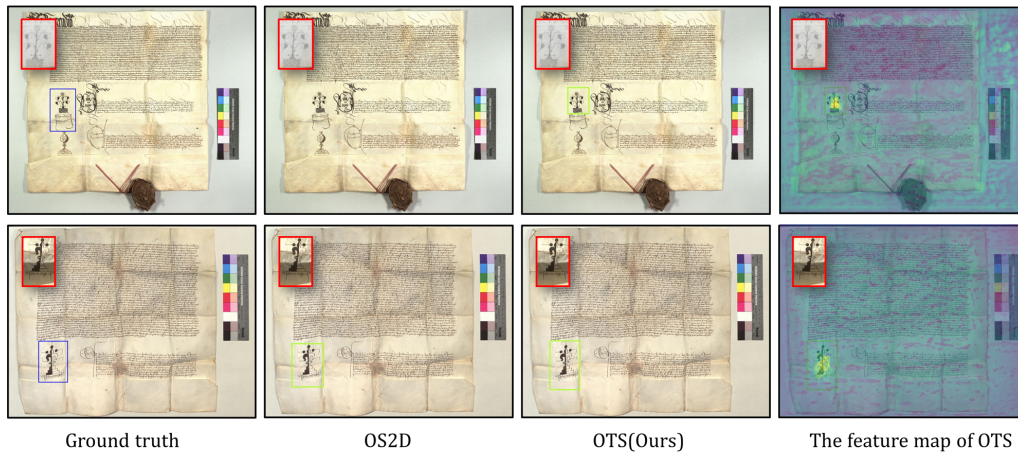


Figure 10: Example results on NC dataset. The leftmost column shows the ground truth, and the red box is the support image. All prediction boxes are shown in green. Best view in color and zoom in.

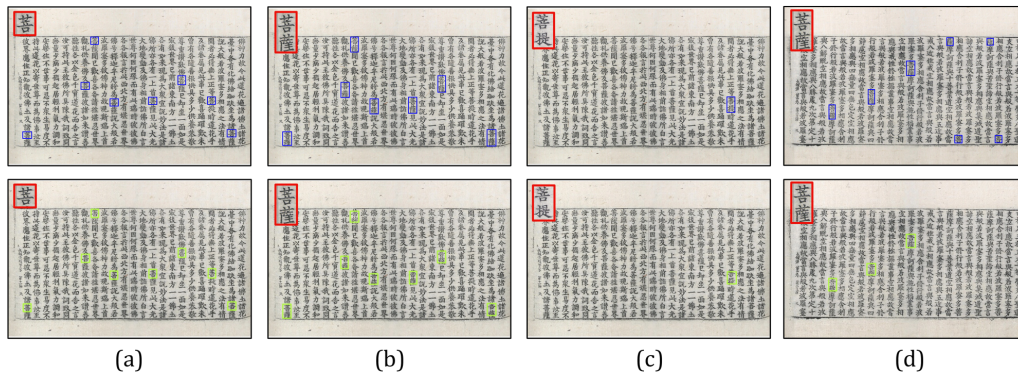


Figure 11: Visualization of the OTS quality. The top row is the ground truth, and the second row is the prediction result of OTS, where the red box is the support image. Best view in color and zoom in.

qualitative experimental results that demonstrate the proposed approach’s efficacy. Notably, our method achieves precise spotting performance for combination characters, as evidenced by the consistent results obtained on the TKH dataset, as depicted in Figure 11. Specifically, Figure 11(b) and Figure 11(c) showcase the performance of the proposed method on combination characters, highlighting its ability to accurately spot novel classes. Nevertheless, our approach may miss instances of novel combination characters with line breaks, as semantic information is lacking, as illustrated in Figure 11(d). It is important to note that users must manually add unseen characters to the

Table 2: Ablation study of feature extractor and test on the DBH Novel. The best results are highlighted in **bold**.

Component	Novel		Base	
	mAP	Recall	mAP	Recall
Res50-ImageNet	99.85	100.0	91.74	95.17
Res50-Synthtext	99.47	98.64	88.58	93.42
Res101-ImageNet	97.03	99.29	86.30	92.88

Table 3: Ablation study of freezing backbone and test on the DBH Novel. The best results are highlighted in **bold**.

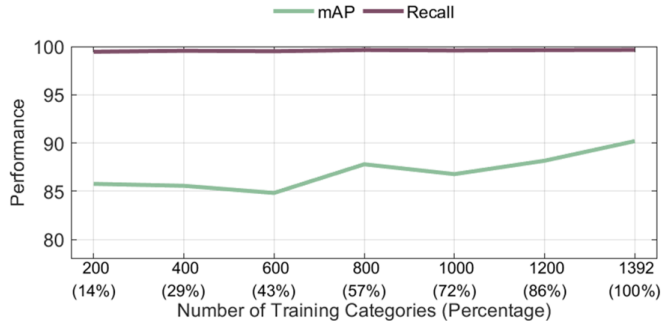
Strategy	Novel		Base	
	mAP	Recall	mAP	Recall
Unfreezing	99.85	100.0	91.74	95.17
Freezing	90.81	98.21	75.75	82.16

support image gallery for novel character classes, as our approach is unable to automatically detect unknown categories in query images. In the future, we aim to explore techniques that dynamically integrate novel characters into the support image gallery, thereby reducing the manual workload.

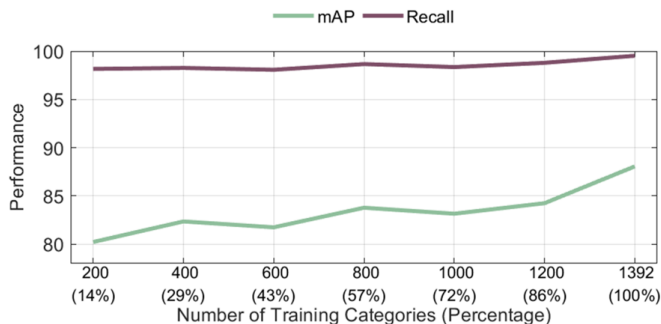
4.4. Ablation Study

4.4.1. Initialization of the feature extractor

When dealing with a scant amount of historical manuscript data, training the network from scratch becomes a challenging task. As evidence by the experimental results present in Table 2, it is apparent that the Resnet-50 backbone pre-trained on ImageNet yields the best performance. Historical manuscripts in different languages may exhibit distinct patterns of texture features. We also tested Resnet-50 pre-trained on the Sythtext dataset [63] as the backbone, which also get high performance. On the other hand, employing the RestNet-101 architecture failed to achieve better results. Based on experimental findings, we select Resnet-50 pre-trained on ImageNet as the backbone for our model. Furthermore, if we freeze the backbone so that it does not perform feature learning, the model also worked quite well, obtaining 90.81% mAP on DBH Novel, see Table 3.



(a) TKH Set 1.



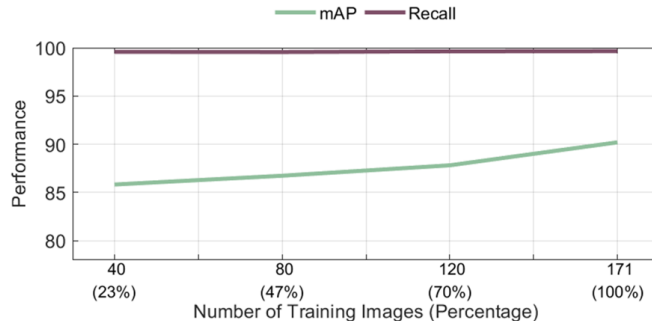
(b) TKH Set 2.

Figure 12: The experiment of subsampling TKH categories during training, and testing on TKH Novel.

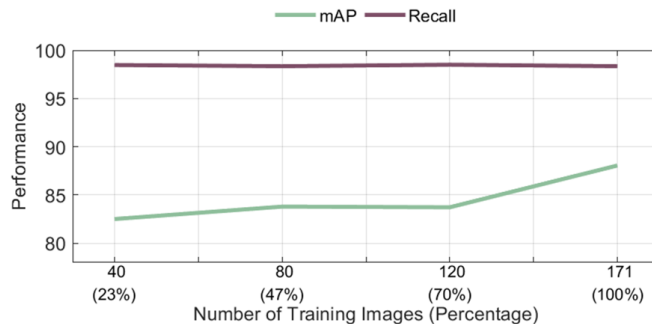
4.4.2. Subsampling Experiment

In contrast to popular object detection datasets such as COCO [65] and VOC [29], historical manuscript images pose unique challenges in terms of smaller sample sizes, a larger number of categories, and significant similarities between categories. To evaluate the effectiveness of our approach in low-resource scenarios, we perform experiments by varying the number of base categories in the training set while keeping the number of input images constant. Figure 12 illustrates the obtained performance scores on the TKH dataset for different numbers of training set categories, ranging from 200 to 1392. As depicted in Figure 12, our results indicate that increasing the number of categories in the training set leads to improved performance, with mAP scores increasing as the number of categories increases, while Recall remains relatively stable.

To explore the impact of the number of input images on the model’s



(a) TKH Set 1.



(b) TKH Set 2.

Figure 13: The experiment of subsampling TKH training images, and testing on TKH Novel.

performance, we further evaluate the model on training sets consisting of 40, 80, 120, and 171 images, corresponding to a total of 1104, 1232, 1320, and 1942 categories, respectively. Our results in Figure 13 demonstrate that increasing the number of input images also positively impacts model performance, as higher mAP scores are observed when more images are used for training, with Recall remaining at a higher level. Consequently, our results demonstrate that augmenting the training data size can improve performance. However, even in low-resource scenarios with a small amount of training data, our method still achieves over 83% of mAP and 95% of Recall scores when trained with only 40 images, as confirmed on the test set with 828 images on the TKH dataset.

In summary, our subsampling experiments confirm the effectiveness of our proposed method in addressing low-resource scenarios. Augmenting the training dataset by either increasing the number of categories or input im-

Table 4: Performance comparison on different attention design methods of OTS on the DBH dataset. The best results are highlighted in **bold**.

Component	Novel		Base	
	mAP	Recall	mAP	Recall
support attention first	99.85	100.0	91.74	95.17
query attention first	98.73	98.93	86.76	89.69
w/o support attention	99.21	100.0	87.89	89.77
w/o query attention	96.10	97.86	89.70	93.45
w/o dual spatial attention block	96.65	99.29	83.80	87.64

ages can lead to improved performance. Even with a limited number of training data, our method achieves high mAP and Recall scores, indicating its robustness and suitability for the spotting of historical manuscripts.

4.4.3. Influence of Attention Design

To empirically validate the efficacy of our proposed framework, we conduct a meticulous ablation study on the dual spatial attention block. Specifically, we perform one of the following operations at a time: (1) interchanging the order of the two spatial attention operations, and (2) removing one of the spatial attention operations. We evaluate all the models on the DBH dataset, and the results are presented in Table 4. The human cognitive process typically involves looking at the support image first and then seeking relevant similar regions on the query image. By altering the order of spatial attention in OTS, with query spatial attention preceding support spatial attention, we observe a decrease in mAP scores by about 0.7% and 3% for the novel and base categories, respectively. The experimental results demonstrate the effectiveness of the proposed module sequence. Removing the spatial attention for support images resulted in a decrease of about 1.7% in mAP scores for the base category, and removing the spatial attention for query images led to about a 3.4% decrease in mAP scores for the novel category, providing evidence that the spatial attention for both support and query images plays a vital role in achieving stable and substantial improvements.

4.4.4. Selection of Loss Function

The loss function constructs from both localization and spotting. For localization, we apply the smooth L_1 loss, and for the spotting loss, to evaluate

Table 5: For testing the spotting loss function, we try several different setting of the loss function in the same architecture. We show the performance on the four dataset with **novel** class. The best results are highlighted in **bold**.

Loss Function	DBH		VML		TKH Set 1		TKH Set 2		NC	
	mAP	Recall	mAP	Recall	mAP	Recall	mAP	Recall	mAP	Recall
Triplet [64]	79.25	86.79	60.00	86.86	71.28	97.75	62.19	95.32	88.83	95.41
Contrastive [57]	92.11	97.14	98.23	98.73	75.79	99.05	69.43	97.48	90.60	94.50
RL [58]	99.47	99.64	98.73	99.58	90.05	99.60	86.99	98.13	90.77	95.72
Torus (Ours)	99.85	100.0	100.0	100.0	90.20	99.65	88.06	99.52	92.14	96.79

the effectiveness of our proposed new loss, we try several different setting of the loss function in the same architecture. Our results in Table 5 show that the triple loss function does not yield meaningful performance, while the contrastive loss function outperforms the triple loss function. The ranked list loss, which can adaptively balance positive and negative samples, obtains good performance. However, the proposed torus loss function outperforms all the other loss functions. This can be attributed to its ability to focus on hard samples in the margin gap and balance positive and negative samples, which facilitates learning distance metrics and promotes text spotting in low-resource scenarios. The experimental results on all four datasets using the torus loss function confirm its superiority compared to other loss functions, thus validating the effectiveness of our proposed approach.

4.4.5. Cross-domain Performance

We have conducted a comprehensive assessment of the cross-domain performance of our proposed model by training it on various datasets and selecting the DBH Novel dataset for testing purposes. The experimental outcomes are presented in Table 6, showcasing the efficacy of our proposed model. For example, when the model is trained on the VML dataset, the DBH Novel dataset can be considered as a novel class. However, the model’s optimal performance is obtained when it is trained and tested on the same dataset, as the data distributions are similar. Nevertheless, cross-domain training may result in a decline in performance, particularly when the data types differ significantly, and a limited number of samples are used in the training process.

Table 6: Cross-domain performance measures of our method when training is done on different datasets and testing on DBH Novel.

Metric	Training Dataset			
	DBH	VML	TKH	NC
mAP	99.85	98.44	92.90	58.23
Recall	100.0	99.29	98.57	61.79

4.5. OTS vs. Human in text spotting

Our approach endeavors to propose a novel model that harnesses the power of pattern recognition techniques to aid researchers in their quest to decipher ancient texts, especially in resource-limited settings.

A user study is conducted to validate the proposed method’s effectiveness in text spotting of historical manuscripts. Eight individuals with bachelor’s degrees or higher are recruited to perform the same tasks as the machine on the test set. To ensure sample independence of the whole experiment, each tester is only allowed to participate once. A between-subjects design is followed, where a support image is configured for each query image, and users spotted as much as possible on the query image based on that support image, a total of 25 images are included, and all images are taken from the DBH, VML, TKH, NC dataset. To motivate testers to perform at their best, additional bonuses are offered to the best performing users (best performance compared with ground truth). Testers’ native language is Chinese, and the test software is available on GitHub⁴.

The results of the experiment are presented in Figure 14. We measured the performance using three metrics, including *Precision*, *Recall* and *F1 score*, where *Precision* denotes the ratio of correct spotting to the total number of spots, and *Recall* denotes the ratio of correct spotting to the ground truth. Furthermore, *F1 score* is the harmonic mean of *Precision* and *Recall*, which provides a comprehensive evaluation of the model’s performance. The average *Precision*, *Recall* and *F1 score* for all testers are 85.62%, 73.75%, and 79.07%, respectively. The OTS method’s performance achieves a *Precision*, *Recall* and *F1 score* of 95.51%, 98.03%, and 96.75%, respectively, and performs better than human spotting through experiments. From the test

⁴<https://github.com/infinite-hwb/ots/tree/master/ST>

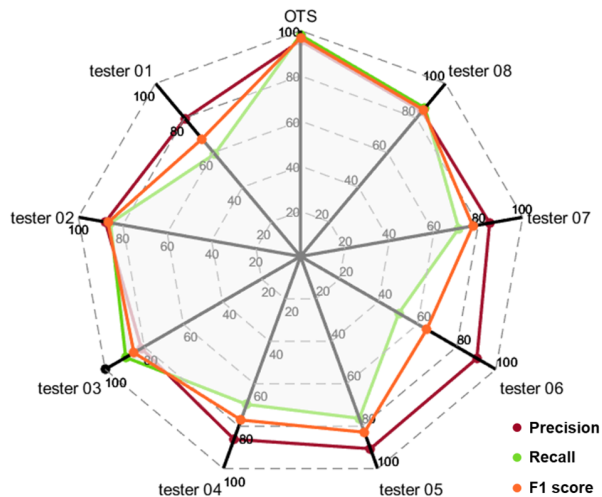


Figure 14: The experiment performance between the human tester and our proposed method. Eight testers are recruited to perform the same tasks as the machine.

result, we notice that testers whose native language is Chinese had difficulty with spotting in Arabic, which is more relevant to the case of novel class spotting, since none of the tester had prior knowledge of Arabic. However, all testers performed well in the Chinese spotting task.

Compared with human spotting, our method significantly reduces the time needed to complete the test items and get the best performance. In terms of time consuming, with less than 2 minutes for our proposed approach compared to an average of 28 minutes for human testers.

5. Conclusions

This paper presents a novel approach for one-shot page-level text spotting in historical manuscripts using deep learning techniques, referred to as OTS, that effectively addresses the low-resource open-set problem. The proposed method leverages dual spatial attention and correlation matching to align support and query images, closely emulating the human cognitive process. The approach enables the spotting of new classes without additional training and is particularly suitable for low-resource scenarios. To address example imbalance, we introduce a novel loss function called torus loss that makes the embedding space of distance metric more discriminative. Our experimental results demonstrate that our approach significantly outperforms existing methods, thereby offering promising applications in this field.

Acknowledgements

This work was supported by the National Key Research and Development Program of China (2020AAA0107903), and the National Natural Science Foundation of China (62176091).

References

- [1] Ma W, Zhang H, Jin L, et al. Joint layout analysis, character detection and recognition for historical document digitization. *International Conference on Frontiers in Handwriting Recognition*, 2020: 31-36.
- [2] Sulaiman A, Omar K, Nasrudin M F. Degraded historical document binarization: A review on issues, challenges, techniques, and future directions. *Journal of Imaging*, 2019, 5(4): 48.
- [3] Yousef M, Bishop T E. OrigamiNet: weakly-supervised, segmentation-free, one-step, full page text recognition by learning to unfold. *Conference on Computer Vision and Pattern Recognition*, 2020: 14710-14719.
- [4] Chung J, Delteil T. A computationally efficient pipeline approach to full page offline handwritten text recognition. *International Conference on Document Analysis and Recognition Workshops*, 2019, 5: 35-40.
- [5] Wicht B, Fischer A, Hennebert J. Deep learning features for handwritten keyword spotting. *International Conference on Pattern Recognition*, 2016: 3434-3439.
- [6] Zagoris K, Pratikakis I, Gatos B. Unsupervised word spotting in historical handwritten document images using document-oriented local features. *IEEE Transactions on Image Processing*, 2017, 26(8): 4032-4041.
- [7] Zagoris K, Amanatiadis A, Pratikakis I. Word spotting as a service: an unsupervised and segmentation-free framework for handwritten documents. *Journal of Imaging*, 2021, 7(12): 278.
- [8] Fujii Y, Driesen K, Baccash J, et al. Sequence-to-label script identification for multilingual ocr. *International Conference on Document Analysis and Recognition*, 2017, 1: 161-168.

- [9] Lee J, Park S, Baek J, et al. On recognizing texts of arbitrary shapes with 2D self-attention. *Conference on Computer Vision and Pattern Recognition Workshops*, 2020: 546-547.
- [10] Sheng F, Chen Z, Xu B. NRTR: A no-recurrence sequence-to-sequence model for scene text recognition. *International Conference on Document Analysis and Recognition*, 2019: 781-786.
- [11] Wang S, Wang Y, Qin X, et al. Scene text recognition via gated cascade attention. *IEEE International Conference on Multimedia and Expo*, 2019: 1018-1023.
- [12] Lake B M, Salakhutdinov R, Tenenbaum J B. Human-level concept learning through probabilistic program induction. *Science*, 2015, 350(6266): 1332-1338.
- [13] Yang H, Jin L, Huang W, et al. Dense and tight detection of chinese characters in historical documents: Datasets and a recognition guided detector. *IEEE Access*, 2018, 6: 30174-30183.
- [14] Bissacco A, Cummins M, Netzer Y, et al. Photoocr: Reading text in uncontrolled conditions. *International Conference on Computer Vision*, 2013: 785-792.
- [15] Xiu Y, Wang Q, Zhan H, et al. A handwritten Chinese text recognizer applying multi-level multimodal fusion network. *International Conference on Document Analysis and Recognition*, 2019: 1464-1469.
- [16] Rothacker L, Sudholt S, Rusakov E, et al. Word hypotheses for segmentation-free word spotting in historic document images. *International Conference on Document Analysis and Recognition*, 2017, 1: 1174-1179.
- [17] Feng W, He W, Yin F, et al. Textdragon: An end-to-end framework for arbitrary shaped text spotting. *International Conference on Computer Vision*, 2019: 9076-9085.
- [18] Qiao L, Tang S, Cheng Z, et al. Text perceptron: Towards end-to-end arbitrary-shaped text spotting. *AAAI Conference on Artificial Intelligence*, 2020, 34(07): 11899-11907.

- [19] Seitzer M, Christlein V. Report: Object retrieval system for historical documents.
- [20] Kesidis A L, Galiotou E, Gatos B, et al. A word spotting framework for historical machine-printed documents. *International Journal on Document Analysis and Recognition*, 2011, 14(2): 131-144.
- [21] Khurshid K, Faure C, Vincent N. Word spotting in historical printed documents using shape and sequence comparisons. *Pattern Recognition*, 2012, 45(7): 2598-2609.
- [22] Zagoris K, Pratikakis I, Gatos B. Segmentation-based historical handwritten word spotting using document-specific local features. *International Conference on Frontiers in Handwriting Recognition*, 2014: 9-14.
- [23] Zhou X, Yao C, Wen H, et al. East: an efficient and accurate scene text detector. *Conference on Computer Vision and Pattern Recognition*, 2017: 5551-5560.
- [24] Shi B, Bai X, Yao C. An end-to-end trainable neural network for image-based sequence recognition and its application to scene text recognition. *IEEE Transactions on Pattern Analysis and Machine Intelligence*, 2016, 39(11): 2298-2304.
- [25] Wang H, Lu P, Zhang H, et al. All you need is boundary: Toward arbitrary-shaped text spotting. *AAAI Conference on Artificial Intelligence*, 2020, 34(07): 12160-12167.
- [26] Liu Y, Chen H, Shen C, et al. Abcnet: Real-time scene text spotting with adaptive bezier-curve network. *Conference on Computer Vision and Pattern Recognition*, 2020: 9809-9818.
- [27] Wang W, Xie E, Li X, et al. Pan++: Towards efficient and accurate end-to-end spotting of arbitrarily-shaped text. *IEEE Transactions on Pattern Analysis and Machine Intelligence*, 2021, 44(9): 5349-5367.
- [28] Wilkinson T, Lindstrom J, Brun A. Neural Ctrl-F: segmentation-free query-by-string word spotting in handwritten manuscript collections. *Proceedings of the IEEE International Conference on Computer Vision*, 2017: 4433-4442.

- [29] Everingham M, Van Gool L, Williams C K I, et al. The pascal visual object classes (voc) challenge. *International Journal of Computer Vision*, 2010, 88(2): 303-338.
- [30] Souibgui M A, Fornés A, Kessentini Y, et al. Few shots are all you need: A progressive learning approach for low resource handwritten text recognition. *Pattern Recognition Letters*, 2022, 160: 43-49.
- [31] Souibgui M A, Fornés A, Kessentini Y, et al. A few-shot learning approach for historical ciphered manuscript recognition. *International Conference on Pattern Recognition*, 2021: 5413-5420.
- [32] Rusu A A, Rao D, Sygnowski J, et al. Meta-Learning with Latent Embedding Optimization. *International Conference on Learning Representations*, 2018.
- [33] Finn C, Abbeel P, Levine S. Model-agnostic meta-learning for fast adaptation of deep networks. *International Conference on Machine Learning*, 2017: 1126-1135.
- [34] Sun Q, Liu Y, Chua T S, et al. Meta-transfer learning for few-shot learning. *Conference on Computer Vision and Pattern Recognition*, 2019: 403-412.
- [35] Oreshkin B, Rodríguez López P, Lacoste A. Tadam: Task dependent adaptive metric for improved few-shot learning. *Advances in Neural Information Processing Systems*, 2018: 719–729.
- [36] Snell J, Swersky K, Zemel R. Prototypical networks for few-shot learning. *Advances in Neural Information Processing Systems*, 2017: 4080–4090.
- [37] Tsutsui S, Fu Y, Crandall D. Reinforcing Generated Images via Meta-learning for One-Shot Fine-Grained Visual Recognition. *Transactions on Pattern Analysis and Machine Intelligence*, 2022.
- [38] Chen Z, Fu Y, Wang Y X, et al. Image deformation meta-networks for one-shot learning. *Conference on Computer Vision and Pattern Recognition*, 2019: 8680-8689.

- [39] Kang B, Liu Z, Wang X, et al. Few-shot object detection via feature reweighting. *International Conference on Computer Vision*, 2019: 8420-8429.
- [40] Osokin A, Sumin D, Lomakin V. Os2d: One-stage one-shot object detection by matching anchor features. *European Conference on Computer Vision*, 2020: 635-652.
- [41] Fan Q, Zhuo W, Tang C K, et al. Few-shot object detection with attention-RPN and multi-relation detector. *Conference on Computer Vision and Pattern Recognition*, 2020: 4013-4022.
- [42] Hsieh T I, Lo Y C, Chen H T, et al. One-shot object detection with co-attention and co-excitation. *Advances in Neural Information Processing Systems*, 2019: 2725–2734.
- [43] Chen D J, Hsieh H Y, Liu T L. Adaptive image transformer for one-shot object detection. *Conference on Computer Vision and Pattern Recognition*, 2021: 12247-12256.
- [44] Perez-Rua J M, Zhu X, Hospedales T M, et al. Incremental few-shot object detection. *Conference on Computer Vision and Pattern Recognition*, 2020: 13846-13855.
- [45] Wang Y X, Ramanan D, Hebert M. Meta-learning to detect rare objects. *International Conference on Computer Vision*, 2019: 9925-9934.
- [46] Yan X, Chen Z, Xu A, et al. Meta r-cnn: Towards general solver for instance-level low-shot learning. *International Conference on Computer Vision*, 2019: 9577-9586.
- [47] Fan Z, Ma Y, Li Z, et al. Generalized few-shot object detection without forgetting. *Conference on Computer Vision and Pattern Recognition*, 2021: 4527–4536.
- [48] Ren S, He K, Girshick R, et al. Faster r-cnn: Towards real-time object detection with region proposal networks. *IEEE Transactions on Pattern Analysis and Machine Intelligence*, 2017, 39: 1137-1149.
- [49] Rocco I, Arandjelovic R, Sivic J. Convolutional neural network architecture for geometric matching. *Conference on Computer Vision and Pattern Recognition*, 2017: 6148-6157.

- [50] Liu Y, Zhu L, Yamada M, et al. Semantic correspondence as an optimal transport problem. *Conference on Computer Vision and Pattern Recognition*, 2020: 4463-4472.
- [51] Zhao D, Song Z, Ji Z, et al. Multi-scale Matching Networks for Semantic Correspondence. *International Conference on Computer Vision*, 2021: 3354-3364.
- [52] Kim J, Ryoo K, Seo J, et al. Semi-Supervised Learning of Semantic Correspondence with Pseudo-Labels. *Conference on Computer Vision and Pattern Recognition*, 2022: 19699-19709.
- [53] Kim S, Min J, Cho M. TransforMatcher: Match-to-Match Attention for Semantic Correspondence. *Conference on Computer Vision and Pattern Recognition*, 2022: 8697-8707.
- [54] Rocco I, Arandjelović R, Sivic J. End-to-end weakly-supervised semantic alignment. *Conference on Computer Vision and Pattern Recognition*, 2018: 6917-6925.
- [55] Jaderberg M, Simonyan K, Zisserman A. Spatial transformer networks. *Advances in Neural Information Processing Systems*, 2015, 2: 2017–2025.
- [56] Radenović F, Tolias G, Chum O. Fine-tuning CNN image retrieval with no human annotation. *IEEE Transactions on Pattern Analysis and Machine Intelligence*, 2018, 41(7): 1655-1668.
- [57] Chopra S, Hadsell R, LeCun Y. Learning a similarity metric discriminatively, with application to face verification. *Conference on Computer Vision and Pattern Recognition*, 2005, 1: 539-546.
- [58] Wang X, Hua Y, Kodirov E, et al. Ranked list loss for deep metric learning. *Conference on Computer Vision and Pattern Recognition*, 2019: 5207-5216.
- [59] Kassis M, Abdalhaleem A, Droby A, et al. Vml-hd: The historical arabic documents dataset for recognition systems. *International Workshop on Arabic Script Analysis and Recognition*, 2017: 11-14.

- [60] Kingma D P, Ba J. Adam: A method for stochastic optimization. *ArXiv preprint*, 1412.6980, 2014.
- [61] He K, Zhang X, Ren S, et al. Deep residual learning for image recognition. *Conference on Computer Vision and Pattern Recognition*, 2016: 770-778.
- [62] Russakovsky O, Deng J, Su H, et al. Imagenet large scale visual recognition challenge. *International Journal of Computer Vision*, 2015, 115(3): 211-252.
- [63] Gupta A, Vedaldi A, Zisserman A. Synthetic data for text localisation in natural images. *Conference on Computer Vision and Pattern Recognition*, 2016: 2315-2324.
- [64] Schroff F, Kalenichenko D, Philbin J. Facenet: A unified embedding for face recognition and clustering. *Proceedings of the IEEE conference on computer vision and pattern recognition*, 2015: 815-823.
- [65] Lin T Y, Maire M, Belongie S, et al. Microsoft coco: Common objects in context. *European Conference on Computer Vision*, 2014: 740-755.